BILINGUAL PUBLISHING GROUP

Journal of Building Material Science

https://journals.bilpubgroup.com/index.php/jbms

ARTICLE

Exploring the Effect of a Cement-Based Self-Healing Additive (CS) on the Durability of Cementitious Materials

Yi Shi*, *Shaoliang Wu*, *Tao Wang*, *Zhenping Shi

Metals and Chemistry Research Institute, China Academy of Railway Sciences, Beijing 100081, China

ABSTRACT

In order to improve the damage resistance of concrete, a cement-based self-healing additive (abbreviate as CS) was prepared. To investigate the influence of CS on the self-healing performance of cementitious material, X-ray diffraction (XRD) and thermal analysis were used to investigate the effects of different dosages of CS on the hydration process and hydration products of cementitious material. Compressive strength test and load damage self-healing test were used to show the influence of different amounts of CS on the mechanical properties of concrete. The pore structure distribution of cement paste with different dosages of CS was analyzed using mercury intrusion testing method. The results indicated that different dosages of CS had no effect on the types of hydration products of cementitious material. Adding an appropriate amount of CS can effectively improve the micro pore structure of cement-based materials, reduce the proportion of harmful pores in the structure, and decrease the most probable pore diameter. When microcracks are generated in the structure under load, CS can promote the formation of hydration products inside the structure to fill the microcracks, thereby improving the self-healing performance of cement-based materials. This study provides an idea for improving microcracks and enhancing durability of marine concrete structures.

Keywords: Cementitious Material; Additive; Self-Healing Performance; Durability; Marine Concrete; Microstructure

*CORRESPONDING AUTHOR:

Yi Shi, Metals and Chemistry Research Institute, China Academy of Railway Sciences, Beijing 100081, China; Email: shiyi0851@qq.com

ARTICLE INFO

Received: 27 April 2025 | Revised: 3 June 2025 | Accepted: 9 June 2025 | Published Online: 9 July 2025

DOI: https://doi.org/10.30564/jbms.v7i3.9720

CITATION

Shi, Y., Wu, S., Wang, T., et al., 2025. Exploring the Effect of a Cement-based Self-healing Additive (CS) on the Durability of Cementitious Materials. Journal of Building Material Science. 7(3): 34–48. DOI: https://doi.org/10.30564/jbms.v7i3.9720

COPYRIGHT

Copyright © 2025 by the author(s). Published by Bilingual Publishing Group. This is an open access article under the Creative Commons Attribution-NonCommercial 4.0 International (CC BY-NC 4.0) License (https://creativecommons.org/licenses/by-nc/4.0/).

1. Introduction

In recent years, the construction of coastal bridge projects has gradually increased [1], and concrete was the commonly used building material. There is much research on the durability of reinforced concrete structures in corrosive environments [2–4]. There is little research on the durability of concrete structures and their appropriate anticorrosion measures in severe corrosion environments, especially in the coastal environment. At present, traditional protection methods such as increasing the thickness of concrete protective layer and coating are mainly used [5,6]. Alternatively, high-performance concrete can be prepared by optimizing material mix proportions, mineral admixtures, and additives to enhance concrete durability. Coatings can emit volatile organic compounds (VOCs) and pollute the environment [7–9]. In the later maintenance process, it is necessary to clean the old coating on the surface, making it difficult to work in the splash zone. At the same time, it pollutes the marine environment and reduces the protective effect. This method cannot repair the damage to the concrete.

A large amount of survey data shows that China also has durability issues that cannot be ignored. The durability problem of building materials in coastal areas is mainly caused by chloride corrosion damage. In the early 1980s, Hong Dinghai, Pan Deqiang, and others investigated hydraulic concrete buildings such as seaports and docks in southern China. The research results show that about 90% of docks suffer structural damage due to concrete cracking and severe corrosion of steel bars. Some overpasses in northern regions have shown damage phenomena such as surface powdering and peeling, freeze-thaw damage, steel corrosion, and cracking along the steel bars. For example, compared to the Xizhimen Overpass in Beijing, which was built and used in 1979, it could not be used until 1999 and had to be demolished and rebuilt [10]. Some scholars have proposed the concept of the "Five-fold Law": if the initial design ignores the requirements of steel reinforcement protection technology and invests less than $1, $5 will be invested in maintenance after the corrosion problem is exposed, and $25 will be spent on reinforcement and repair after the concrete surface of the protective layer cracks along the reinforcement. Finally, when the structure is severely damaged, the maintenance cost will be as high as $125 [11]. It can be seen that the durability of concrete is an urgent and pressing global problem that needs to be solved urgently.

Marine concrete is faced with a very complex environment. One is that soluble salts such as chlorides and sulfates [12–15], which are abundant in seawater, cause chemical corrosion to concrete [16]. The other is that concrete located in the tidal zone of the ocean is accelerated by dry wet cycles. When a load is applied to concrete, the micro-cracks inside the concrete increase [17], and these micro-cracks expand and connect with each other, forming transmission channels, making it easier for corrosive media to enter. The combined effect of the above multiple destructive factors will greatly accelerate the deterioration of concrete [18–20]. There are also many examples of premature erosion and damage to structures in coastal areas of our country, especially coastal structures built before the 1980s, where 50% of them were damaged in less than 10 years of use. Almost all ports in northern China suffer from varying degrees of concrete freeze-thaw damage, with carbonation causing a decrease in the alkalinity of the concrete, and steel bars losing their protective layer and passivation film, leading to corrosion. The Cl^- causes corrosion of steel bars, leading to cracking of concrete protective layers and premature failure of structures, which is also very common in marine engineering in China. Concrete bridges built across the sea and coastal areas are exposed to harsh marine environments, and the durability of the structures is a concern due to steel corrosion. The economic losses caused by corrosion of concrete structures in China exceed billions. In 2014, the cost of structural anti-corrosion repair in China was about 2.1278 trillion-yuan, accounting for 3.34% of China's total annual GDP. Each Chinese person bears an average annual loss of about 1,555 yuan for structural anti-corrosion repair. Therefore, it is very important to study the deterioration law and mechanism of concrete in marine environment.

There are various ways to improve the durability of concrete. Among them, high-performance concrete has good compactness and a good cementitious pore structure, good impermeability and frost resistance, and high electrical resistivity. But strict requirements are placed on the selection of raw materials and construction control, and

there is a high degree of self-shrinkage and brittleness [21]. Marine concrete has strong resistance to seawater corrosion, good freeze-thaw resistance, low hydration heat, but low early strength and slow strength development. At the same time, it is sensitive to the selection of additives such as water reducing agents or pumping agents. Corrosion inhibitors can increase the chloride ion resistance of the passive film on steel bars in offshore structures, and increase the critical chloride ion content for steel bar corrosion. However, rust inhibitors are expensive and have weak targeting for key areas of steel bars [22]. Increasing the thickness of the concrete protective layer can effectively prevent steel corrosion, but there is a certain limit to its thickness increase [23]. When the protective layer is too thick, it will reduce the load-bearing capacity of the structure. In summary, marine concrete structures need to find a more cost-effective and less demanding method to improve the overall durability of the pattern.

The most severely corroded structures in marine engineering are located at the splash zone. The splash zone is not only affected by tides for a long time in a dry-wet cycle environment, but also by the mechanical force of splashing waves. To further improve the performance of concrete structures in the splash zone, this paper intends to systematically study the durability of concrete. This study aims to investigate the influence of CS on the durability performance of cement-based materials in terms of microstructure, mechanical properties, etc., thereby finding ideas for improving the durability of hydraulic structures.

2. Experimentation

2.1. Materials

The chemical composition of reference cement (C) produced by China Academy of Building Materials Science and Technology Co., Ltd. and cementitious admixture (CS) produced by Metals and Chemistry Research Institute, China Academy of Railway Sciences is shown in **Table 1**. The mixing water is deionized water. CS is in the form of solid powder, with silica at the nanoscale.

Table 1. Chemical Composition of Materials/%.

Composition	SiO_2	Al_2O_3	Fe_2O_3	CaO	MgO	SO_3	Na_2O_{eq}	f-CaO	Loss
C	22.37	4.36	3.38	61.08	2.43	2.45	0.506	0.86	1.33
CS	21.33	12.52	3.51	38.23	22.33	-	-	0.36	1.72

2.2. Methods

2.2.1. X-Ray Diffraction (XRD)

X-ray diffraction (XRD) analysis was performed using a PANalytical X'Pert PRO instrument (PANalytical, Almelo, Netherlands), equipped with a Cu Kα radiation source and a nickel foil filter. X-rays are a form of electromagnetic radiation with short wavelengths (ranging from 0.06 to 20 nm) that can penetrate materials of certain thicknesses and induce fluorescence in specific substances, as well as cause light sensitivity in photographic film or gas ionization. In crystalline materials, when the crystal is positioned at varying angles relative to the incident beam, crystal planes that meet the Bragg diffraction condition are detected, resulting in diffraction peaks of varying intensity in the XRD pattern.

Dried cement paste was placed on a flat plate sample geometry. A fixed divergence slit of 1/16 degree was chosen to limit beam overflow on the samples at small angles of 2θ. The X'Celerator high-speed linear detector was used for the XRD experiment, and scans ranged from 5 to 70 degrees [24,25].

2.2.2. Thermogravimetric Analysis (TG)

TG/DTG was done by used METTLER TOLEDO TGA 2 thermal analyzer (METTLER TOLEDO, Zurich, Switzerland). The instrument used for thermogravimetric analysis is called a thermogravimetric analyzer, which mainly consists of three parts: temperature control system, detection system, and recording system. Micro commercial thermogravimetric analysis, also known as derivative thermogravimetric analysis, can be derived from thermogravimetric analysis. It is a technique for recording the first derivative of TG curves with respect to temperature or time. Thermogravimetric analysis can be used to detect physical and chemical changes. It can be seen that these physical

and chemical changes involve mass changes, such as sublimation, vaporization, adsorption, desorption, absorption, and gas-solid reactions.

A ceramic crucible containing dried cement paste was subjected to heating from ambient temperature up to 1050°C, with a heating rate of 10°C/min. This process was carried out under a nitrogen gas flow of 70 mL/min [26–32].

2.2.3. Scanning Electron Microscope (SEM)

During this stage, the samples were analyzed using the SEM technique (Tescan Mira4) to investigate their microstructural characteristics. Scanning electron microscopes function differently compared to optical microscopes. Instead of relying on reflected light, these microscopes feature an electron gun at the top of the instrument that generates electrons under high voltage and directs them toward the sample. These electrons scan the surface of the specimen, causing the displacement of electrons from the object's surface. The electrons emitted from the object's surface, referred to as Secondary Electrons (SE), are detected by the device's sensor, which then forms an image. This system is capable of producing highly precise images of the specimen's surface. The device is linked to a monitor that displays the SE images, which are particularly effective for assessing surface roughness and revealing cracks and cavities [33].

Scanning electron microscopy (SEM) serves as an observational method that bridges transmission electron microscopy and optical microscopy. A key advantage of SEM is its versatility in handling diverse sample types, with minimal risk of damaging or contaminating the original specimen. Furthermore, it enables the simultaneous acquisition of morphological, structural, compositional, and crystallographic data.

2.2.4. Mercury Intrusion Porosimetry

Mercury Intrusion Porosimetry (MIP) can measure pores ranging from 10nm to 200um, which can be used to analyze the pore size distribution of pores that have a significant impact on the performance of hardened cement mortar. The mercury intrusion method involves pressing mercury into dried slurry samples at different pressures, where the pores in the slurry are cylindrical and have the following relationship [34]:

$$p \times \pi r^2 = -2\pi r \times \sigma \cos \vartheta \quad (1)$$

where p–the applied pressure, MPa

θ–the wetting angle of mercury on solids generally varies between 135–142;

σ– the surface tension of mercury is 484.2 (48.42Pa) at 25 °C;

r–the radius of capillary pores(Å•)

In the formula (1), 2σcosθ is generally approximated as −7500 (MPa•Å), resulting in r=7500/p(Å). This means that under pressure p, mercury has already been injected into any hole greater than r. Therefore, as long as the measured hole pressure is obtained, the minimum radius of the hole that can be penetrated under this pressure can be calculated. After changing the pressure, r can be measured again. Raise the pressure from p_1 to p_2, measure the pore sizes r_1 and r_2, and then try to measure the volume of mercury ΔV per unit weight of the sample pressed between the pores with diameters r_1 and r_2. Finally, by continuously changing the pore pressure, the amount of mercury entering different levels of pores can be measured, thus obtaining the pore size distribution of the sample. At present, structurally similar dilatometers are used to measure mercury intrusion volume using capacitance, height, or resistance methods.

2.2.5. Compressive Strength

Cement, rubble (diameter 5–20mm, as a coarse aggregates), river sand, water, and additives were mixed according to ratio. Concrete mixer (Wuxi Jian Gong Test Equipment Co., Ltd., Wuxi, China) was used: mix sand and aggregate together for 120s, then add cement and admixtures and mix for another 120s. Finally, add water and mix for 120s before molding. The sample (150 mm× 150 mm×150 mm) was kept in a horizontal position (temperature 20 ± 2 ℃, relative humidity above 95%) in molds for 24 h at different temperatures. They were then extracted and moved to a standard curing room until testing time. The compressive strength tests were conducted on the specimens cured for 3, 7, and 28 days according to GB/T 50081-2019 [35,36]. The maximum pressure that a cubic specimen can withstand per unit area. Three identical samples were tested for each test, and the values were averaged.

2.2.6. Self-Healing Performance Test

Cure (20±2°C, RH ≥ 95%) each group (**Table 2**) of concrete specimens for 28 days, retain 3 of them each group as comparison specimens for further curing, and proceed to the next step of testing for the other specimens. Load the specimen with 80% compressive strength for 20 seconds, unload and continue cure until 56 days. Then, conduct compressive strength tests with the comparison specimen. Calculate the compressive strength recovery rate and self-healing ability according to the following formula [37–40].

$$\eta=\frac{f_c}{f_0}\times 100\% \quad (2)$$

where η–compressive strength recovery rate,
f_c–compressive strength of pre-compressed specimens, MPa
f_0–comparative compressive strength of comparison specimens, MPa

$$R_c=\frac{\eta_s}{\eta_c}\times 100\% \quad (3)$$

where R_c–load damage self-healing ability ratio, %
η_s–recovery rate of compressive strength after self-healing of concrete load damage, %
η_c–recovery rate of compressive strength after self-healing of concrete load damage of comparison specimens, %

Table 2. Concrete Proportion (by Mass).

Composition	Cement	Sand	Aggregate	Water	Admixture, %
C-0	1	2.1	2.1	0.43	0
CS-1	1	2.1	2.1	0.43	1
CS-2	1	2.1	2.1	0.43	2
CS-3	1	2.1	2.1	0.43	3

3. Results and Discussions

Prepare cement paste for microscopic tests, with the mix proportion as shown in **Table 3**. Prepare concrete specimens for strength test and load damage self-healing test. The mix proportion is shown in **Table 2**.

Table 3. Cement Paste Proportion (by Mass).

Composition	**Cement**	**Water**	**Admixture, %**
Control	1	0.31	——
CS-5%	1	0.31	5
CS-10%	1	0.31	10
CS-20%	1	0.31	20

3.1. Hydration Products

3.1.1. X-Ray Diffraction (XRD)

In order to analyze the effect of CS dosage on the hydration products of cement paste at different ages, this study conducted XRD test on the hydration products at different stages (**Figure 1**). The X-ray diffraction analysis results are shown in the **Figure 1(a)** and **(b)**.

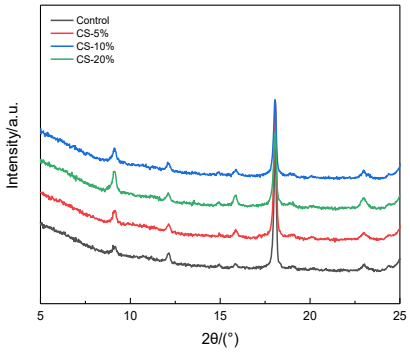

(a) 7d

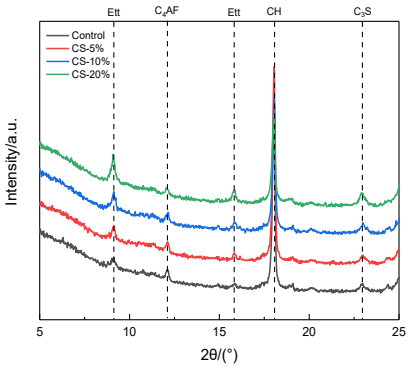

(b) 28d

Figure 1. CS XRD Pattern of Cement Paste. **(a)** 7d. **(b)** 28d.

As shown in **Figure 1**, characteristic peaks such as calcium hydroxide (CH), tetracalcium aluminate (C_4AF), and tricalcium silicate (C_3S) are clearly present at every age. **Figure 1** shows the peaks of ettringite (Ett), calcium hydroxide (CH), tetracalcium aluminate (C_4AF), and tricalcium silicate (C_3S) which are the main hydration products of cement. Calcium silicate is an inorganic compound with the molecular formula Ca_3SiO_5. It is one of the components of cement. The hydration reaction of tricalcium silicate is fast and releases a large amount of heat during hydration. Pure tricalcium silicate is only stable within the temperature range of 1250–2065 °C. It melts inconsistently

into calcium oxide and liquid phase above 2065 ℃, and decomposes into dicalcium silicate and calcium oxide below 1250 ℃. Under rapid cooling conditions, the decomposition rate of tricalcium silicate is slow, allowing it to exist in a metastable state at room temperature. Tricalcium silicate can be generated by solid-state reaction between calcium oxide and silicon dioxide at high temperatures, or by reaction between dicalcium silicate and calcium oxide. Tricalcium silicate is the main mineral in cement clinker, with a content of up to 50% or more. Etringite is a colorless to yellow calcium aluminum sulfate mineral, typically in the form of colorless columnar crystals that turn white upon partial dehydration. Swelling is the biggest characteristic of ettringite, and the hydration of CaO, Al_2O_3, and $CaSO_4$ in cement to form ettringite can increase the solid phase volume by about 120%.

The hydration products of the cement paste after adding CS are consistent with them. It indicates that CS doesn't hinder or alter the formation of the final hydration products of cement, and on the other hand, the hydration products formed by CS itself are consistent with those of cement. With the increase of CS content, the characteristic peaks of cement clinker such as C_4AF and C_3S increased slightly. As the age increases, the peak of CH significantly increases, indicating that the addition of CS does not inhibit the formation of calcium hydroxide during cement hydration process. The phase peak of another important cement hydration product, Ett, also becomes more pronounced with increasing age. The clinker content of group 0 cement at the same age is lower and the hydration degree is higher, which suggests that the high dosage of CS may slow down the hydration rate of cement.

3.1.2. Thermogravimetric Analysis (TG)

To further investigate the effect of CS on cement hydration, thermogravimetric analysis (TG/DTG) was used to analyze the hydration process of cementitious materials in group 0 and the other groups at different ages (**Figure 2**). The TG/DTG curves are shown in **Figure 2(a)** and **(b)**.

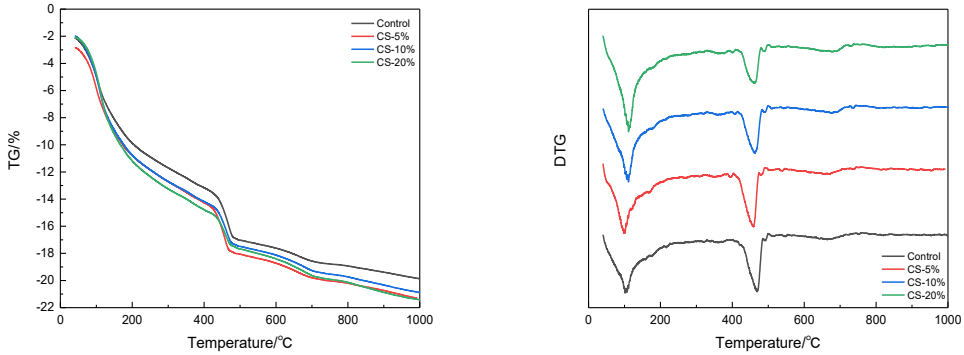

(a) 7d TG/DTG

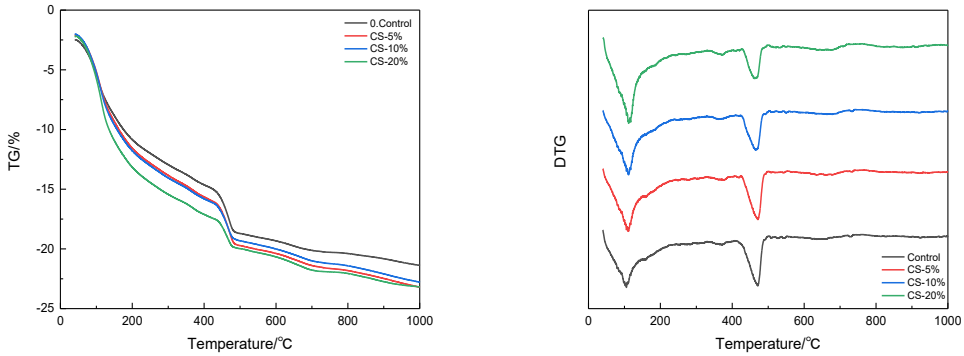

(b) 28d TG/DTG

Figure 2. CS TG/DTG Curves. **(a)** 7d TG/DTG. **(b)** 28d TG/DTG.

The TG curve shows the decrease in the quality of cement paste hardening products when burned from room temperature to 1000 ℃, and the content of various phases can be calculated from the degree of mass reduction in different temperature segments. It is generally believed that the decrease in mass from room temperature to 105 ℃ mainly reflects the content of free water in the specimen. 350–500℃ is the decomposition temperature of $Ca(OH)_2$ under heat. When the temperature rises to near 800℃, the chemically bound water in the cement paste has been decomposed by heat. The DTG is the slope of the TG, and the temperature range of mass reduction judged by the DTG curve is more obvious. The core principle of TG analysis is to monitor the quality changes of the sample in real-time under program temperature control through a high-precision balance. During the testing process, the sample is placed in a specific atmosphere (such as nitrogen or oxygen) and heated or cooled at a constant rate. The quality change data is recorded in real-time and plotted as a TG curve. The weight loss step of the TG curve corresponds to processes such as material decomposition and oxidation, while the DTG curve reflects the peak rate of weight change through differential calculations. The results of thermogravimetric analysis are related to experimental conditions. In order to obtain accurate and reproducible thermogravimetric curves, it is necessary to carefully analyze various influencing factors.

From **Figure 2(a)**, it can be seen that at the 7 days, all experimental groups with added CS lost more weight, indicating a higher content of free water in the slurry. The weight loss was rapid from room temperature to 105 ℃, and this trend became more pronounced with the increase of CS content. Correspondingly, during the thermal decomposition stage of Ca $(OH)_2$, the blank group lost more weight and had a higher degree of hydration. The results in **Figure 3** show that as the age increases, the CH content in each group of cement slurry gradually increases. At the same age, adding an appropriate amount of CS (not exceeding 5% in this section) can promote the generation of CH, but excessive CS may delay the early hydration of cement. The addition of CS has little effect on the content of chemically bound water in cement samples, and may exist in an amorphous form in the samples.

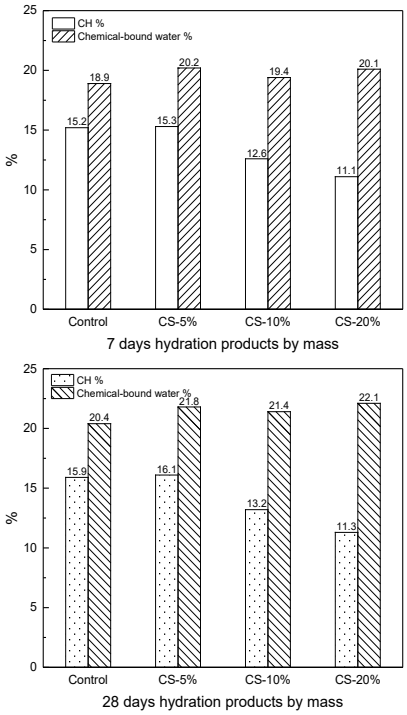

Figure 3. Hydrate Content Calculated from TG Test.

3.1.3. Scanning Electron Microscope (SEM)

A total of eight SEM images were chosen for the image processing analysis (**Figure 4**). The key details regarding the SEM image samples are presented in **Figure 4(a)–(h)**. In recent years, the application of SEM in concrete research has gained increasing recognition. Owing to significant advancements in concrete technology, numerous researchers have conducted extensive studies using SEM to investigate the microstructure of concrete [41–45].

According to **Figure 4**, adding CS to cement paste can effectively improve the consistency of the paste. From **Figure 4**, it can be seen that for the same water cement ratio, in the early stage of hydration, there are fewer hydrates, and the gaps between solid phases (cement particles) inside the slurry are larger, resulting in a larger hydration space. Hydrates are generally identifiable. With the passage of hydration time, hydrates continuously fill the voids, and the hydration voids shrink continuously. Finally, hydrates interweave or bond together, making it impossible to identify individual hydrate particles. The CSH gel in the sample at the center of the inner layer of the cement sample will not grow into large-sized hydrates due to the restriction of the external hydrated layer. In addition, the CSH gel tends to be in the form of closely packed short

needles where the hydration space is very small. From **Figure 4**, it is observed that there is a layer of fine ettringite on the surface of cement particles during the initial hydration stage. However, during the setting period, the fine ettringite disappears and is replaced by coarse ettringite crystals, resulting in a decrease in the number of crystal particles. At 7 days, the surface of the control group specimens was rough with obvious pores. Due to the low level of early hydration, the pores in the specimens had not yet been filled with hydration products. The experimental group with CS during the same period showed fewer pores at the same magnification, with a dark gray dense surface, and began to form hydration products to fill the pores. At 28 days, with the increase of age, the surface of each group gradually becomes smooth and dense. A small amount of spinel structure can be observed in the cracks of the blank group, considering that it is a complex of hydration products such as Ett and C-S-H gel. When observing the experimental groups with added CS, it was noted that the CS-5% group had a smooth and compact surface, while the CS-10% and CS-20% groups had larger pores filled with hydration products. Various hydration compounds intertwined within these pores, forming complex clusters without forming dense hydration products. From the above, it can be seen that CS can effectively improve the consistency of cement specimens with appropriate dosage, which will contribute to the improvement of concrete durability performance in the splash zone.

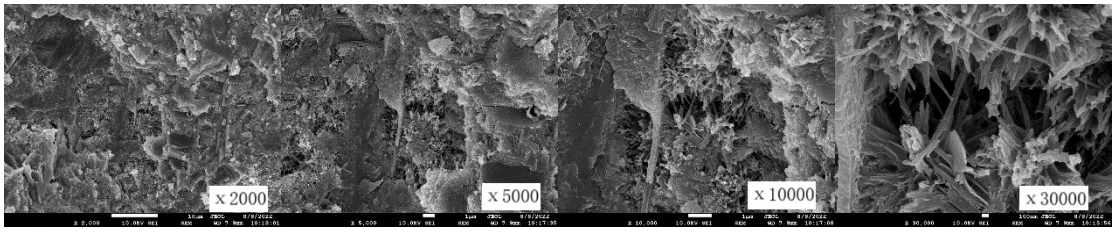

(a) 7d Control

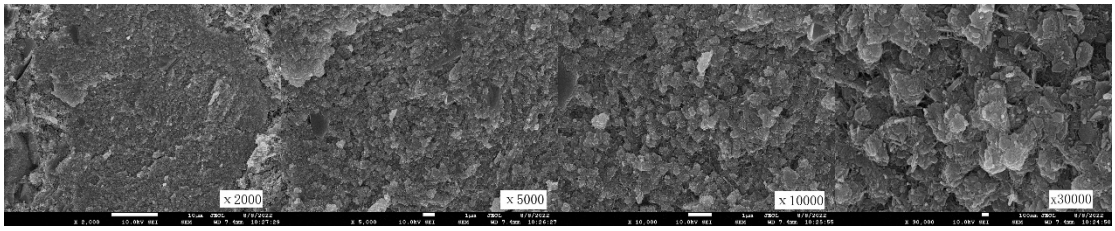

(b) 7d CS-5%

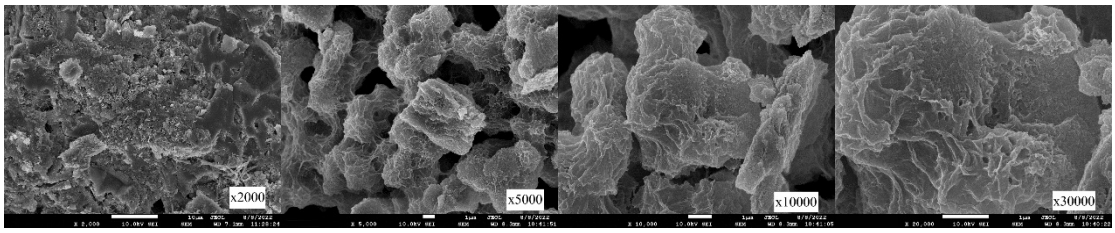

(c) 7d CS-10%

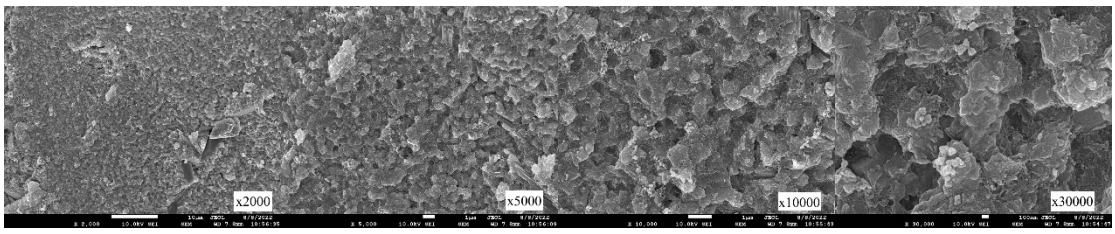

(d) 7d CS-20%

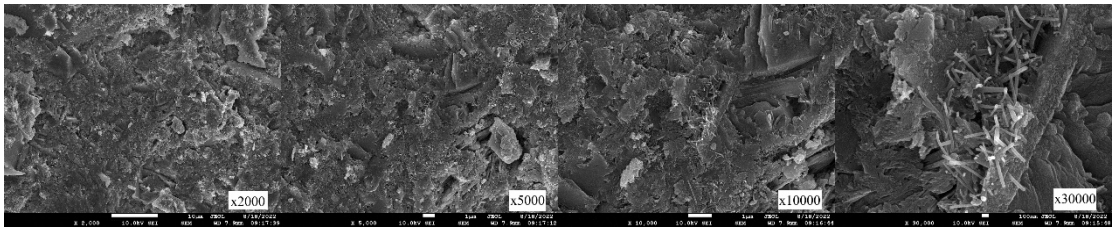

(e) 28d Control

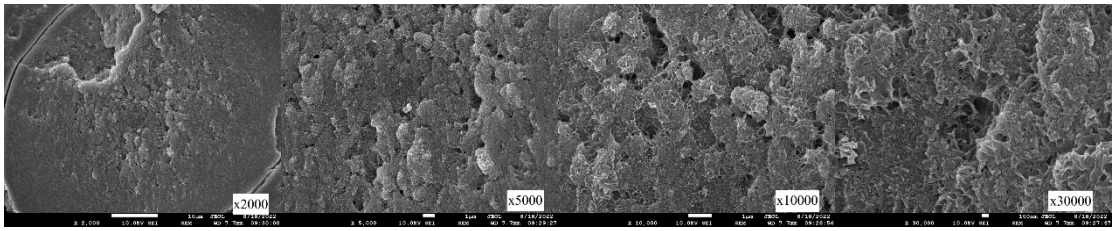

(f) 28d CS-5%

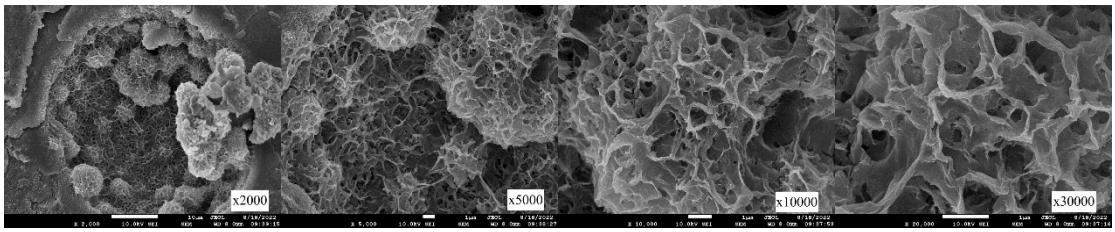

(g) 28d CS-10%

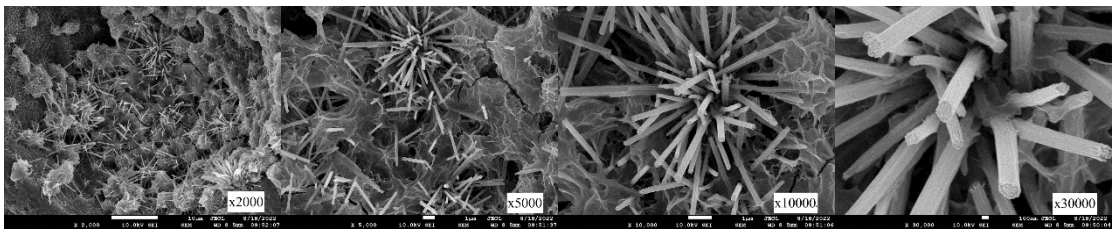

(h) 28d CS-20%

Figure 4. Microscopic Morphology of Cement in Different Experimental Groups at Different Ages. **(a)** 7d Control. **(b)** 7d CS-5%. **(c)** 7d CS-10%. **(d)** 7d CS-20%. **(e)** 28d Control. **(f)** 28d CS-5%. **(g)** 28d CS-10%. **(h)** 28d CS-20%.

Figure 5 shows a comparison photo of the microstructure between the control group and the 5% CS group at 28 days (**Figure 5(a)** and **(b)**). It can be seen that there are small cracks in the internal microstructure of the control group at 28 days. Taking the sample at this point as an example, the maximum width of the micro cracks is 4–5nm. At the same magnification, the hydration products of the experimental group with 5% CS added are more tightly cross-linked, and there are few micro cracks. Even if there are micro cracks, they are filled and wrapped by the cross-linked hydration products. According to the EDS spectrum results (**Figure 6**), the experimental group with added CS produced a large amount of hydrated calcium silicate and hydrated calcium aluminate (**Figure 6(a)** and **(b)**), which effectively filled the micro cracks in the structure itself.

3.1.4. Mercury Intrusion Porosimetry

The Mercury Intrusion Porosimetry is currently the most widely used and effective method for studying pore size distribution. In order to investigate the effect of proliferating agents on the internal pore structure of hydration products, mercury intrusion porosimetry was used to test and analyze the effect of different dosages of CS agents on the internal pore structure of clean slurry specimens at different ages (**Figure 7**).

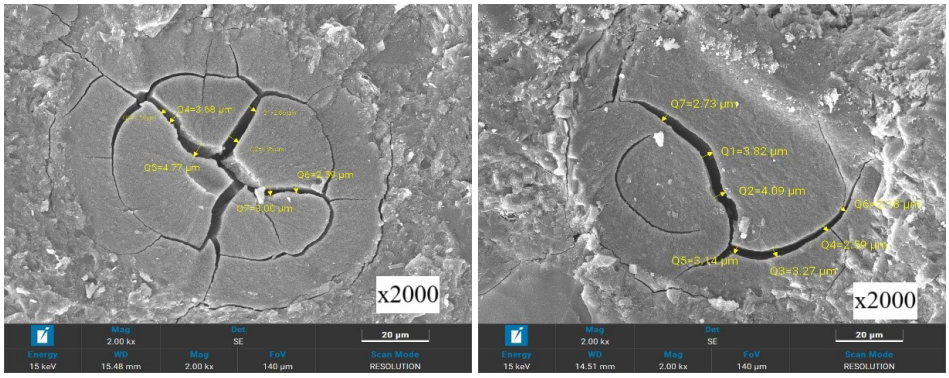

(a) Microscopic Crack Size of Control Group

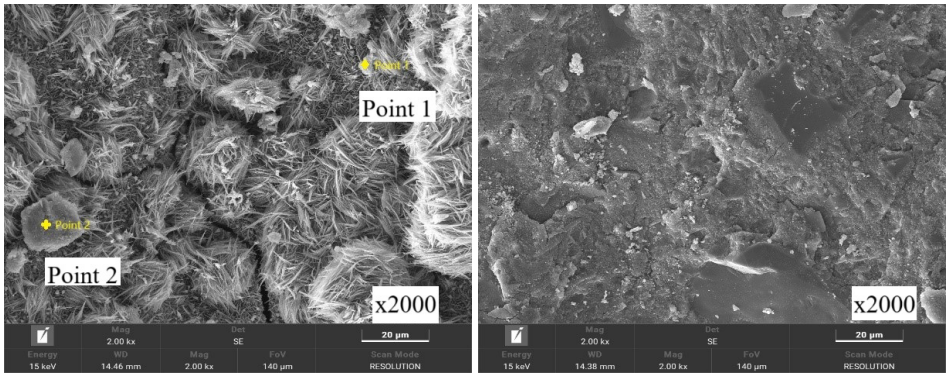

(b) 5% CS Group Microstructure

Figure 5. Comparison of Microstructure Between Experimental Groups with and Without CS at the Same Magnification. **(a)** Microscopic Crack Size of Control Group. **(b)** 5% CS Group Microstructure.

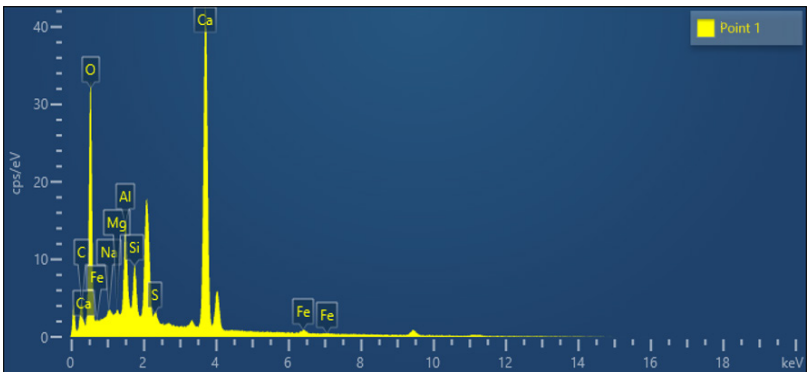

(a) EDS Spectrum at Point 1

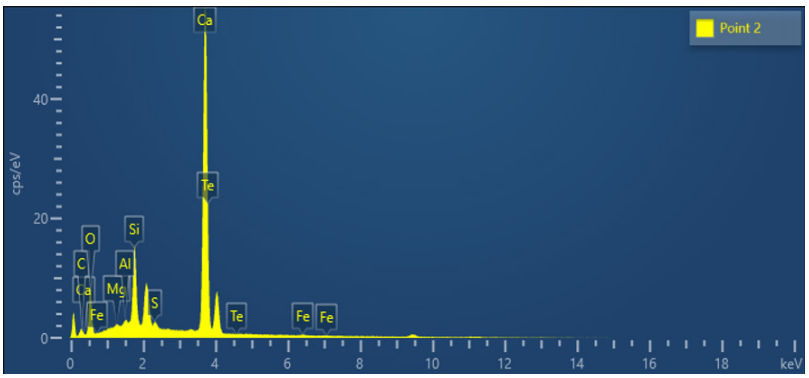

(b) EDS Spectrum at Point 2

Figure 6. EDS Spectra at Points 1 and 2. **(a)** EDS Spectrum at Point 1. **(b)** EDS Spectrum at Point 2.

As shown in **Figure 7(a)–(d)**, the effect of adding different amounts of CS on the pore size distribution inside the cement slurry is slightly different. The pores in concrete can be divided into four categories: ultra-micropores ($r \leq 5$ nm); micropores (5 nm < r < 100 nm); large capillary pores (100nm≤r<1000nm); non capillary pores (1000nm ≤ r) [46]. The overall trend is that with the introduction of the additive and the increase of the dosage, the most-probable pore diameter of the hydration product of the purified slurry gradually decreases. Within the micro pore range, the smaller the pore size, the better the frost resistance, crack resistance, and atmospheric stability of the structure. When CS is added to cement slurry, the most-probable pore diameter of the control group at 7 days of age is around 45nm, while the most most-probable pore diameter of the CS-10% and CS-20% experimental groups is only 25–30nm. However, the differential curves of the experimental group with CS additive showed multiple peaks, which may be due to the high dosage of additive and incomplete hydration of the additive powder, resulting in a certain range of pore size distribution. As the age increases, CS powder gradually participates in hydration, and the differential curve becomes smoother with a single peak. Only when the CS dosage is 20%, the differential curve shows a double peak, which is consistent with the macroscopic characteristic of slow hydration of the slurry under high dosage. At 28 days of age, the most-probable pore diameter of the CS-5% and CS-10% experimental groups were almost equal to those of the control group. The differential curve of the CS-20% experimental group showed a double peak, which may be related to the decrease in hydration rate caused by the high dosage of CS. From the integral curve, it can be seen that at both 7 and 28 days, the experimental group with added CS showed a characteristic of more small pore sizes. Especially at 28d, the experimental group with added 20% CS showed a significant increase in the total volume of small pores, indicating that CS can effectively reduce the most probable pore size in the slurry and increase the proportion of small pore sizes in all pores. When the most probable pore size of cement-based materials is less than 100nm, the smaller the pore size, the better the overall frost resistance, crack resistance, and durability of the structure. It can be seen that adding an appropriate amount of CS can improve the internal pore structure of cement-based materials.

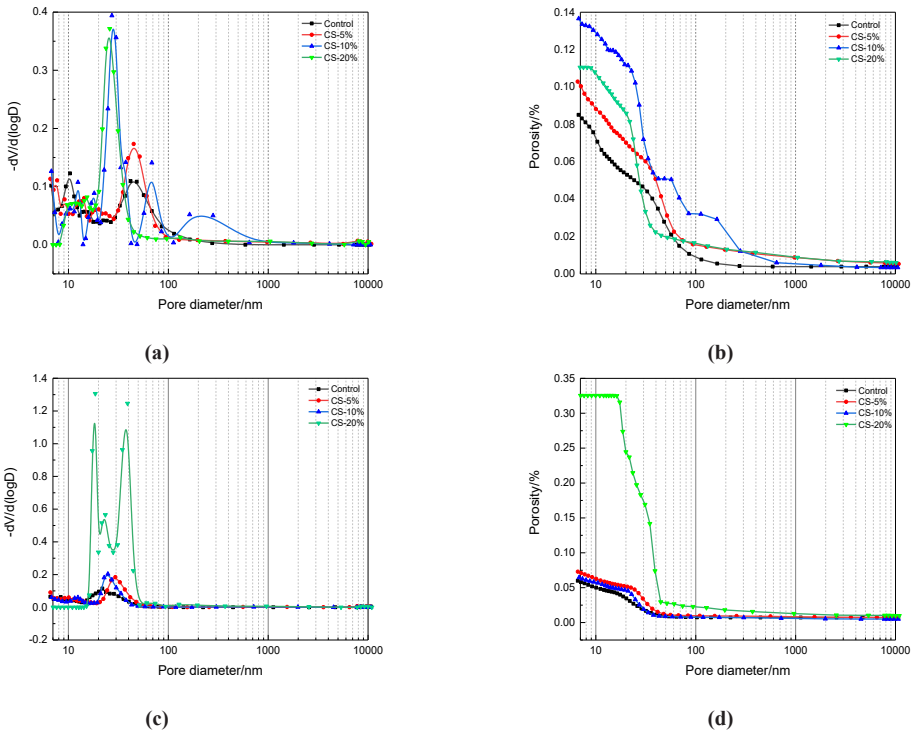

Figure 7. Mercury Intrusion Porosimetry Curve of Net Slurry. **(a)** 7d Differential Curve of Pore Size Distribution. **(b)** 7d Integral Curve of Pore Size Distribution. **(c)** 28d Differential Curve of Pore Size Distribution. **(d)** 28d Integral Curve of Pore Size Distribution.

3.2. Compressive Strength

Based on the above micro test results, consider reducing the CS content to prepare concrete, with the mix as shown in **Table 2**. The compressive strength of concrete is shown in **Figure 8**.

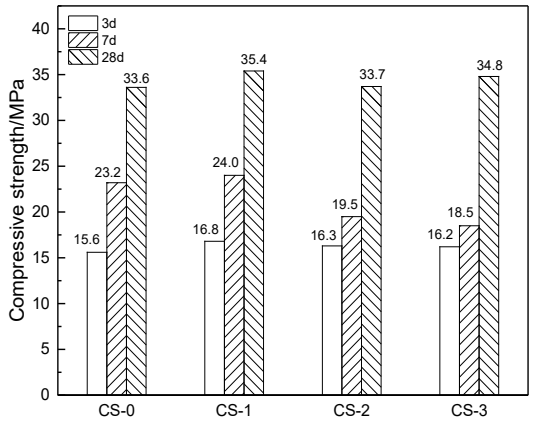

Figure 8. Compressive Strength.

It can be seen from **Figure 8** that the compressive strength of each experimental group with CS admixture gradually increases with the increase of age, and the strength of the control group is similar to that of the experimental group at 3d. At 3 days of age, the compressive strength of the concrete in the test group with a CS content of 1% was the highest at 16.8MPa, which was 8% higher than the compressive strength of the control group at the same age. The difference in compressive strength between the experimental groups with added CS is relatively small. The experimental group with a dosage of 3% has the lowest compressive strength, but still has a higher compressive strength than the control group. At 7 days, the strength of experimental groups decreased slightly with the increase of CS content. The performance of each experimental group mixed with CS is not the same. The compressive strength of the concrete test group with a CS content of 1% is 24MPa, which is 0.8MPa higher than the control group. The compressive strength of the experimental group with a dosage of 3% increased slowly, with a 7d strength of only 18.5MPa, which was 20% lower than the control group. The compressive strength increased rapidly within the period of 7 to 28 days, and there was no difference between the experimental groups and the control group. With the increase of age, the compressive strength of experimental groups showed different changes. The CS-1 group continued to maintain the same level as the CS-0 group, and the CS-2 and CS-3 groups decreased slightly. The compressive strength of concrete test groups with CS content of 2% and 3% increased rapidly between 7 and 28 days. Compared to the 7-day intensity, the CS-2 experimental group showed a 73% increase in 28 day intensity; The compressive strength of CS-3 test group 28 increased by 88%. The above data indicates that CS with a dosage greater than 1% may affect the early compressive strength of concrete, but it is also beneficial for the growth of later strength. The experimental group with a 1% dosage added to the 28 days compressive strength had the highest value, reaching 35.4 MPa, which was 1.8 MPa higher than the control group.

3.3. Self-Healing Performance

To visually compare the effect of CS additives on the self-healing performance of concrete, this study conducted a self-healing test on concrete load damage, and the results are as follows (**Figure 9**).

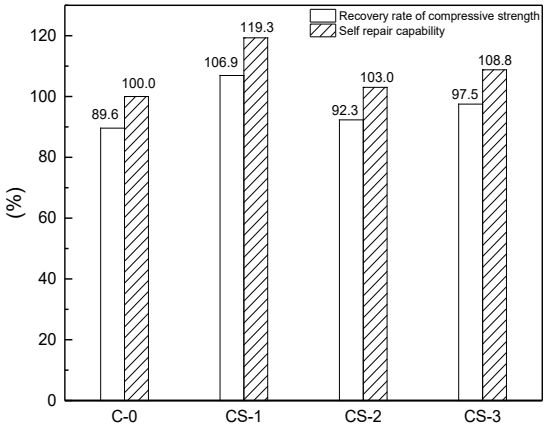

Figure 9. Concrete Self-Healing Performance.

The sample is subjected to preloading treatment, and the mortar specimen is subjected to preloading treatment using an integrated universal testing machine for compressive and flexural strength, with the aim of causing cracks inside the specimen and simulating the generation of microcracks in concrete under load in real use environments. As shown in **Figure 9**, the compressive strength recovery rate of experimental groups doped with CS were higher than those of the blank group. Among them, the CS-1 group had the highest value, 19% higher than that of the control group. The compressive strength recovery rate

of the CS-2 experimental group was 3% higher than that of the control blank group. The compressive strength recovery rate of the CS-3 experimental group was 9% higher than that of the control group. The load damage self-healing ability ratio of concrete samples with added CS is significantly improved. The load damage self-healing ability ratio of CS-1 group concrete specimens is as high as 119.3%. The self-healing ability of the CS-2 test group in the concrete test group with added CS was the lowest at 103%, but still higher than the control group. CS admixtures can keep the self-healing ability of concrete above 100% in the content of 1.0%–3.0%, and the addition of 1% CS can significantly improve the self-healing ability of concrete.

4. Conclusions

(1) CS does not form harmful substances in cement and does not affect the types of hydration products in cement-based materials. CS with a dosage higher than 5% will apparently prolong the jelling time of cement-based materials and affect their early strength.

(2) CS with a dosage of less than 3% does not affect the compressive strength of concrete at 28 days and the effect is better when the dosage is 1%.

(3) CS with a dosage of less than 3% can improve the compressive strength recovery rate and self-healing ability of concrete. A 1% CS content can increase the compressive strength recovery rate and self-healing ability of concrete by 19.3%, and effectively improve the compressive strength of concrete after damage. It is suggested that CS can be added together with dry materials during the concrete mixing process and used in structures such as bridge piers and offshore pipe piles to extend the service life of the structure and improve its overall durability.

Author Contributions

Conceptualization, Y.S. and T.W.; methodology, Y.S.; software, Z.S.; validation, S.W. and Z.S.; formal analysis, Y.S.; investigation, S.W.; resources, T.W.; data curation, Z.S.; writing—original draft preparation, Y.S.; writing—review and editing, Y.S.; visualization, T.W.; supervision, S.W.; project administration, T.W.; funding acquisition, T.W. All authors have read and agreed to the published version of the manuscript.

Funding

This work was supported by China Academy of Railway Sciences grant number [No.2023YJ078].

Institutional Review Board Statement

Not applicable.

Informed Consent Statement

Not applicable.

Data Availability Statement

All data in this article has been displayed in the main text, with no other hidden data.

Acknowledgments

Thank you to all the authors. Thank you to the Metals and Chemistry Research Institute, China Academy of Railway Sciences for providing the laboratory and equipment.

Conflicts of Interest

The authors declare no conflict of interest. The funders had no role in the design of the study; in the collection, analyses, or interpretation of data; in the writing of the manuscript; or in the decision to publish the results.

References

[1] Ting, M.Z.Y., Wong, K.S., Rahman, M.E., et al., 2021. Deterioration of marine concrete exposed to wetting-drying action. Journal of Cleaner Production. 278, 123383. DOI: https://doi.org/10.1016/j.jclepro.2020.123383

[2] Fan, Q., Fan, L., Quach, W.M., et al., 2023. Application of microbial mineralization technology for marine concrete crack repair: A review. Journal of Building Engineering. 69, 106299. DOI: https://doi.org/10.1016/j.jobe.2023.106299

[3] Ragab, A.M., Elgammal, M.A., Hodhod, O.A., et al., 2016. Evaluation of field concrete deterioration under real conditions of seawater attack. Construction and Building Materials. 119, 130–144.

[4] Vera, R., Villarroel, M., Carvajal, A.M., et al., 2009. Corrosion products of reinforcement in concrete in marine and industrial environments. Materials Chemistry and Physics. 114(1), 467–474.

[5] Wong, L.S., 2015. Microbial cementation of ureolytic bacteria from the genus Bacillus: a review of the bacterial application on cement-based materials for cleaner production. Journal of Cleaner Production. 93, 5–17. DOI: https://doi.org/10.1016/j.jclepro.2015.01.019

[6] Stocks-Fischer, S., Galinat, J.K., Bang, S.S., 1999. Microbiological precipitation of CaCO3. Soil Biology and Biochemistry. 31(11), 1563–1571. DOI: https://doi.org/10.1016/S0038-0717(99)00082-6

[7] Gollapudi, U.K., Knutson, C.L., Bang, S.S., et al., 1995. A new method for controlling leaching through permeable channels. Chemosphere. 30(4), 695–705.

[8] Qian, C., Ren, L., Xue, B., et al., 2016. Bio-mineralization on cement-based materials consuming CO2 from atmosphere. Construction and Building Materials. 106, 126–132.

[9] Ferris, F.G., Phoenix, V., Fujita, Y., et al., 2004. Kinetics of calcite precipitation induced by ureolytic bacteria at 10 to 20°C in artificial groundwater. Geochimica et Cosmochimica Acta. 68(8), 1701–1710.

[10] Hong, N., 2000. Analysis and Countermeasures of Winter Salt Spraying in Northern China [in Chinese]. Proceedings of the 5th National Symposium on Building Corrosion Protection [in Chinese]; 8 September 2000; Beihai City, China. pp. 17–20.

[11] Xue, B., Sun, Q., Wang, C., et al., 2017. Research status and prospects of corroded reinforced concrete structures [in Chinese]. China Energy and Environmental Protection [in Chinese]. 4, 174–179.

[12] De Muynck, W., Cox, K., De Belie, N., et al., 2008. Bacterial carbonate precipitation as an alternative surface treatment for concrete. Construction and Building Materials. 22(5), 875–885.

[13] Ramezanianpour, A.A., Ghoreishian, S.A.H., Ahmadi, B., et al., 2018. Modeling of chloride ions penetration in cracked concrete structures exposed to marine environments. Structural Concrete. 19(5), 1460–1471.

[14] Ormellese, M., Berra, M., Bolzoni, F., et al., 2006. Corrosion inhibitors for chlorides induced corrosion in reinforced concrete structures. Cement and Concrete Research. 36(3), 536–547. DOI: https://doi.org/10.1016/j.cemconres.2005.11.007

[15] Balapour, M., Hajibandeh, E., Ramezanianpour, A., 2018. Engineering properties and durability of mortars containing new nano rice husk ash (RHA). In: Hordijk, D., Luković, M. (eds.). High Tech Concrete: Where Technology and Engineering Meet. Springer: Cham, Switzerland. pp. 199–206.

[16] Qian, C., Wang, J., Wang, R., et al., 2009. Corrosion protection of cement-based building materials by surface deposition of CaCO3 by Bacillus pasteurii. Materials Science and Engineering: C. 29(4), 1273–1280. DOI: https://doi.org/10.1016/j.msec.2008.10.025

[17] De Muynck, W., Debrouwer, D., De Belie, N., et al., 2008. Bacterial carbonate precipitation improves the durability of cementitious materials. Cement and Concrete Research. 38(7), 1005–1014. DOI: https://doi.org/10.1016/j.cemconres.2008.03.005

[18] Zahedi, M., Ramezanianpour, A.A., Ramezanianpour, A.M., 2015. Evaluation of the mechanical properties and durability of cement mortars containing nanosilica and rice husk ash under chloride ion penetration. Construction and Building Materials. 78, 354–361.

[19] Cavaco, E.S., Neves, L.A.C., Casas, J.R., 2017. Reliability-based approach to the robustness of corroded reinforced concrete structures. Structural Concrete. 18(2), 316–325.

[20] Hossain, M.M., Karim, M.R., Hasan, M., et al., 2016. Durability of mortar and concrete made up of pozzolans as a partial replacement of cement: A review. Construction and Building Materials. 116, 128–140. DOI: https://doi.org/10.1016/j.conbuildmat.2016.04.147

[21] An, M., Zhu, J., Qin, W., 2001. The self-shrinkage problem of high-performance concrete [in Chinese]. Journal of Building Materials [in Chinese]. 6, 159–166.

[22] Zhu, Y., Cai, W., Li, S., et al., 2015. Electrical migrating inhibiting technology of rebar corrosion inhibitor [in Chinese]. Port & Waterway Engineering [in Chinese]. 4, 37–40.

[23] Xu, H., Hao, S., Zhang, J., 2020. Control of thickness of concrete protective layer [in Chinese]. Highway Transportation Technology (Applied Technology Edition) [in Chinese]. 16(11), 120–122.

[24] Naber, C., Stegmeyer, S., Jansen, D., et al., 2019. The PONKCS method applied for time resolved XRD quantification of supplementary cementitious material reactivity in hydrating mixtures with ordinary Portland cement. Construction and Building Materials. 214, 449–457.

[25] Kupwade-Patil, K., Palkovic, S.D., Bumajdad, A., et al., 2018. Use of silica fume and natural volcanic ash as a replacement to Portland cement: Micro and pore structural investigation using NMR, XRD, FTIR and X-ray microtomography. Construction and Building Materials. 158, 574–590.

[26] Soin, A.V., Catalan, L.J., Kinrade, S.D., 2013. A combined QXRD/TG method to quantify the phase composition of hydrated Portland cements. Cement and Concrete Research. 48, 17–24.

[27] Vedalakshmi, R., Raj, A.S., Srinivasan, S., et al., 2003. Quantification of hydrated cement products of

blended cements in low and medium strength concrete using TG and DTA technique. Thermochimica Acta. 407(1–2), 49–60. DOI: https://doi.org/10.1016/S0040-6031(03)00286-7

[28] Slanika, T., Madej, T., Jakubekov, D., 1985. DTA contribution to study of hydration fly ash-Portland cement pastes. Thermochimica Acta. 93, 601–604.

[29] Monzo, J., Paya, J., Borrachero, M.V., et al., 2001. Fluid catalytic cracking residue (FC3R) as a new pozzolanic material: Thermal analysis monitoring of FC3R/Portland cement reactions. Proceedings of the Seventh CANMET/ACI International Conference on Fly Ash, Silica Fume, Slag and Natural Pozzolans in Concrete; 11 May 2001; Madras, India. Supplementary Volume, pp. 22–27.

[30] Sha, W., Pereira, G.B., 2001. Differential scanning calorimetry study of normal Portland cement paste with 30% fly ash replacement and of the separate fly ash and ground granulated blast furnace slag powders. Proceedings of the Seventh CANMET/ACI International Conference on Fly Ash, Silica Fume, Slag and Natural Pozzolans in Concrete; 11 May 2001; Madras, India. Supplementary Volume, pp. 295–309.

[31] Justnes, H., Ostnor, T., 2001. Pozzolanic, amorphous silica produced from the mineral olivine. Proceedings of the Seventh CANMET/ACI International Conference on Fly Ash, Silica Fume, Slag and Natural Pozzolans in Concrete; 11 May 2001; Madras, India. 2, pp. 769–782.

[32] Bhatty, J.I., Dollimire, D., Gamlen, G.A., et al., 1986. Estimation of calcium hydroxide in OPC. Thermochimica Acta. 106, 115–123.

[33] Ahamad, M.S., Maizul, E.N.M., 2020. Digital analysis of georeferenced concrete. Civil and Environmental Engineering Reports. 30(2), 65–79.

[34] Gao, Y., Wu, K., Yuan, Q., 2021. Limited fractal behavior in cement paste upon mercury intrusion porosimetry test: Analysis and models. Construction and Building Materials. 276, 122231. DOI: https://doi.org/10.1016/j.conbuildmat.2020.122231

[35] GB/T 17671-1999. 1999. Method of Testing Cement-Determination of Strength. China Quality and Standards Publishing & Media Co., Ltd.: Beijing, China.

[36] EN 1992-1-1:2004. 2004. Design of concrete structures.

[37] T/CECS 913-2021. 2021. Standard for test method of self-healing performance of cement concrete. China Association for Engineering Construction Standardization: Beijing, China.

[38] ISO 9597:2008. 2008.Cement-Test methods-Determination of setting time and soundness. International Organization for Standardization: Geneva, Switzerland.

[39] ISO 3696:1987. 1987. Water for analytical laboratory use-Specification and test methods. International Organization for Standardization: Geneva, Switzerland.

[40] ISO 679:2009. 2009. Cement-Test methods-Determination of strength. International Organization for Standardization: Geneva, Switzerland.

[41] Weerheijm, J. (ed.), 2013. Introduction to concrete: a resilient material system. In: Weerheijm, J. (ed.). Understanding the Tensile Properties of Concrete. Woodhead Publishing Series in Civil and Structural Engineering. Woodhead Publishing: Cambridge, UK. pp. 1–14.

[42] Scrivener, K., Snellings, R., Lothenbach, B., 2016. A Practical Guide to Microstructural Analysis of Cementitious Materials. CRC Press: Boca Raton, FL, USA.

[43] Giannuzzi, L., 2018. Scanning Electron Microscopy and X-Ray Microanalysis, 4th ed. Springer: New York, NY, USA.

[44] Leite, M., Monteiro, P., 2016. Microstructural analysis of recycled concrete using x-ray microtomography. Cement and Concrete Research. 81, 38–48.

[45] Adili, E., Riginejad, M., 2021. Analyzing the effect of micro rubber, micro SiO2, and nano SiO2 in microcracks in self-consolidating concrete (SEM observation). Civil Engineering Journal. 7(1), 107–117. DOI: https://doi.org/10.28991/cej-2021-03091641

[46] Chen, L., 2007. The influence of concrete pore size on its service life [in Chinese]. Journal of Wuhan University of Technology [in Chinese]. 29(6), 50–53.